Biosensors and Bioelectronics 201 (2022) 113980

Contents lists available at ScienceDirect

Biosensors and Bioelectronics

journal homepage: www.elsevier.com/locate/bios

Electrochemiluminescent emission potential tunable Cu–Zn–In–S/ZnS nanocrystals for multiplex microRNAs potential-resolved detection

Yang Jiang, Qian Li, Yun Xu, Wanqiao Bai, Xia Yang, Sijia Li, Yan Li *

Key Laboratory of Synthetic and Natural Functional Molecule Chemistry of the Ministry of Education, College of Chemistry and Materials Science, Northwest University, Xi'an, Shaanxi, 710069, PR China

ARTICLE INFO

Keywords:
Electrochemiluminescence
Nanocrystal
Simultaneous detection
MicroRNA

ABSTRACT

The development of a multi-target simultaneous detection electrochemiluminescence (ECL) strategy remains a great research interest, however, the limited choice of ECL luminophores is the main limitation holding the field back. In this study, a band gap tunable Cu–Zn–In–S/ZnS nanocrystals (CZIS/ZnS NCs) was synthesized and applied to a potential-resolved ECL detection strategy. By changing the Cu ratio in the precursor, the CZIS/ZnS NCs ECL emission spectrum and emission potential were tuned from 480 to 750 nm and −2.10 to −1.11 V, respectively. In addition, an ECL biosensor was fabricated with CZIS/ZnS NCs as signal reporters to detect three types of microRNAs, which could sensitively and selectively determine microRNA-21, microRNA-141, and microRNA-155 in a single cathodic ECL process. The results showed that the ECL intensity was directly linear to the logarithm of the concentration of microRNA-21, microRNA-141, and microRNA-155 from 0.00001 to 10 nM with detection limits of 2.2, 2.6, and 2.7 fM, respectively. This study demonstrates that the emission potential tunable CZIS/ZnS NCs can be employed as a promising alternative to the toxic II-V and II-V NCs to simultaneously detect multiple disease markers, and can guide the further rational design of both ECL luminophores and multi-analyte ECL sensors.

1. Introduction

Electrochemiluminescence (ECL), a newest generation proven diagnostic technique after chemiluminescence and photoluminescence (PL) (Cao et al., 2020; Qi and Zhang, 2020), has been widely used in biomedical diagnostics and detection because of its high on-board stability and sensitivity, wide dynamic range, and most importantly almost zero-background signal (Ma et al., 2020). However, multiplex analyte detection in a single run ECL process is still limited in this field because of narrow choice of ECL luminophores (Guo et al., 2018; Wang et al., 2021b; Zhou et al., 2018). Because the occurrence and development of diseases are commonly associated with the abnormalities in multiple biomarkers (Jones et al., 2020; Ma and Liu, 2015), multi-target simultaneous detection is an unavoidable challenge in the ECL field. At present, multiple ECL signals in simultaneous detection strategies usually come from spatially-resolved array or multiplex ECL luminophores at one electrode with intensity-based wavelength-resolved or potential-resolved (Deiss et al., 2009; Han et al., 2014; Jones et al., 2020; Lv et al., 2020; Zhang et al., 2019b; Zhou et al., 2018; Zou et al., 2017). In the former case, an expensive ECL imaging reader instrument and microscopically integrated spot arrays are required (Pakchin et al., 2017). Without the ECL imaging reader and sophisticated microcosmic ECL spot arrays, macroscopic ECL arrays is essentially equivalent to multiple continuous ECL analysis process. In the latter case, the wavelength-resolved model also needs to be coupled with high-cost spectrometer and the already weak ECL signal will attenuate further through the optical splitting system. In contrast, the potential-resolved model does not require sophisticated instruments or high throughput ECL signal (Wang et al., 2021b). However, owing to the difficulty in regulating the emission potential of ECL luminophores, potential-resolved ECL signals mostly come from two ECL luminophores that emit light at the cathode and cathode, respectively (Babamiri et al., 2018; Feng et al., 2015; Zhou et al., 2017). This inevitably introduces a multiplex coreactant and electrochemical process, which inevitably causes an undesired interferences reaction between the electrochemical intermediates of each ECL luminophore or coreactant produced during cathodic and anodic electrochemical process. Therefore, the development of a potential-resolved ECL system within a single cathode or anode ECL process will simplify these complex systems and is still an attractive and challenging research interest.

* Corresponding author.
E-mail address: yanli@nwu.edu.cn (Y. Li).

https://doi.org/10.1016/j.bios.2022.113980
Received 8 December 2021; Received in revised form 5 January 2022; Accepted 6 January 2022
Available online 8 January 2022

Luminescent colloidal nanocrystals (NCs) , also known as quantum dots (QDs), have attracted significant great attention in the ECL field over the past two decades because of their unique optoelectronic properties such as high fluorescence (FL) quantum yield (Φ_{FL}), narrowband emission and tunable band gap (Knowles et al., 2016; Owens and Brus, 2017; Wu and Yan, 2013). Unfortunately, the most commonly used electrochemiluminescent II-V and II-V QDs in biological application suffer from disadvantages such as containing highly toxic elements (Cd, Hg, Pb, Se, Te, etc.) and require extremely hazardous and costly precursors (Pu et al., 2016; Zhang et al., 2011, 2014). As a promising candidate, I-III-VI and I-II-III-VI semiconductor NCs such as Cu–In–S and Cu–Zn–In–S (CZIS) have been successfully applied in ECL recently due to their avoidance of disadvantages, as described above (Sun et al., 2018; Zhang et al., 2019a). Since the bulk band gaps of ZnS, In_2S_3, and Cu_2S respectively are 3.7, 2.1, and 1.1 eV, respectively, such a big gap between each monocase sulfide bulk led the band gap of Cu–Zn–In–S/ZnS NCs can be tuned on a large scale (approximately 2.5 eV) by changing the proportions of each component (Coughlan et al., 2017; Li et al., 2011; Pan et al., 2008; Stroyuk et al., 2018). This is a viable approach for developing NCs based emission-potential tunable ECL luminophores.

The development of potential-resolved ECL methods for multiplex target detection remains rather limited at present, particularly in a single cathodic or anodic ECL process for the simultaneous detection of three or more analytes. The crucial issue for the successful fabrication of multiplexed ECL signal sensors is the preparation of ECL emitters with different emission potentials. In this study, a Cu–Zn–In–S/ZnS NCs (CZIS/ZnS NCs) based potential-resolved ECL system was proposed for the first time, in which ECL emission potential tunable CZIS/ZnS NCs (−1.11, −1.68, and −2.10 V vs Ag/AgCl) was synthesized with various stoichiometries by using low-cost and non-toxic commercial precursors (copper (I) iodide, zinc acetate, indium acetate, and sulfur powder see Experimental Section). ZnS shell coated on Cu–Zn–In–S core is a non-toxic and stable semiconductor material. Due to its high lattice matching with the Cu–Zn–In–S core, it can effectively eliminate some surface defects and isolate the effect of water and oxygen on ECL (Cao et al., 2020; Zhang et al., 2019a).

MicroRNA (miRNA), a type of microcosmic and abundant noncoding RNA, play a crucial role in post-transcriptional regulation of gene expression, and their abnormal expression is related to many diseases (leukemia, diabetes, cancers, and cardiovascular disease, etc.) (Bartel, 2018; Gebert and MacRae, 2019; Thorsson et al., 2018; Treiber et al., 2019). However, the sensitive and multiple detection of miRNAs is still challenging because of their ultralow concentration, low molecular weight, susceptibility to degradation, and high sequence homology among miRNA family members (Liu et al., 2019; Ye et al., 2019; Zhang et al., 2020). In recent years, a series of ECL biosensors have been implemented to achieve high sensitivity detection of miRNAs, however, simultaneous detection of multiple miRNAs at a single cathodic or anodic ECL process has not yet been reported.

In this study, a highly sensitive and selective ECL biosensor for the simultaneous detection of three target microRNAs (miRNA-21, miRNA-141, and miRNA-155) was developed using hairpin DNA as the recognition element and three kinds of CZIS/ZnS NCs (with ECL emission potential at −1.11, −1.68, and −2.10 V vs Ag/AgCl) as the ECL signal producing reporter at a single cathode ECL process. The ECL probes were prepared by bonding the three kinds of aminated and carboxylated CZIS/ZnS NCs separately with three different aminated hairpin DNAs tagged with ferrocene (NH_2-HDNA1-Fc, NH_2-HDNA2-Fc and NH_2-HDNA3-Fc). The amination and carboxylation of CZIS/ZnS NCs were performed by modifying the glutathione and mercaptopropionic acid on the surface of the CZIS/ZnS NCs. Fc was used as an efficient ECL quencher of CZIS/ZnS NCs, and was assigned as probe 21, probe 141, and probe 155 to recognize miRNA-21, miRNA-141, and miRNA-155. The ECL biosensor was fabricated by bonding the three probes with chitosan (CS) modified glassy carbon electrode (GCE) via glutaraldehyde (GA). In the absence of target miRNAs, the three different hairpin probes were in a folded configuration in which Fc was held in close proximity to the surface of the electrode, allowing the generation of a weak ECL signal. In the presence of target miRNA-21, miRNA-141, and miRNA-155, the stem-loop of the ECL probes on the electrode were converted into a linear double-helix configuration due to hybridization, resulting in the Fc moving away from the electrode surface, which in turn increased the ECL signal. The strong ECL emission of CZIS/ZnS NCs at −1.11, −1.68, and −2.10 V vs Ag/AgCl was recovered due to different hairpin DNA probes is opened and Fc separated with different CZIS/ZnS NCs. The ECL emission tunable CZIS/ZnS NCs as ECL reporter will open up an important avenue for the development of novel nontoxic element NC ECL luminophores. Moreover, the successful simultaneous detection of three kinds of miRNAs in a single cathodic ECL process might promote the accurate diagnosis and classification of diseases.

2. Experimental section

2.1. Reagents and materials

Materials: Sulfur powder (99.99%), zinc acetate ($Zn(OAc)_2$, 99.99%), copper (I) iodide (CuI, 99.99%), indium acetate ($In(OAc)_3$, 99.99%), dodecanethiol (DDT, 99.9%), L-glutathione (GSH, 95%), mercaptopropionic acid (MPA, 98%), oleylamine (OAm, 97%), N, N-dimethylformamide (DMF, 99.9%), octadecene (ODE, 90%), tetramethylammonium hydroxide (TMAOH, in MeOH, 25 wt %), glutaraldehyde (GA), chitosan (CS, in acetic acid, 0.5 wt %), 6-mercapto-1-hexanol (MCH), ethyl acetate (EA, 99.7%), potassium ferricyanide ($[Fe(CN)_6]^{3-/4-}$, 99.9%), hexane, acetone, 1-(3-Dimethylaminopropyl)-3-ethylcarbodiimide hydrochloride (EDC, 99.9%) and N-hydroxysuccinimide (NHS, 99.9%) were all obtained from Shanghai Macklin Biochemical Co., Ltd (Shanghai, China). DNA and microRNA (miRNA) sequences were customized from Sangon Biotech Co., Ltd (Shanghai, China). Ultrapure water was obtained from a Millipore water purification system (specific resistance of 18 MΩ cm, Milli-Q, Millipore) and was used throughout this study.

Oligonucleotide sequences:

NH_2-HDNA1-Fc:5′–NH_2–$(CH_2)_5$-CGG TTC TAT CAA CAT CAG TCT GAT AAG CTA TAG AAC CG–$(CH_2)_6$–Fc-3′

NH_2-HDNA2-Fc:5′–NH_2–$(CH_2)_5$-CGG TTC TAC CAT CTT TAC CAG ACA GTG TTA TAG AAC CG–$(CH_2)_6$–Fc-3′

NH_2-HDNA3-Fc:5′–NH_2–$(CH_2)_5$-CGG TTC TAC CCC TAT CAC GAT TAG CAT TAA TAG AAC CG–$(CH_2)_6$–Fc-3′

miRNA-21: 5′-UAG CUU AUC AGA CUG AUG UUG A-3′

miRNA-141: 5′-UAA CAC UGU CUG GUA AAG AUG G-3′

miRNA-155: 5′-UUA AUG CUA AUC GUG AUA GGG G-3′

2.2. Synthesis of CZIS/ZnS NCs

For a typical synthesis, CuI (1.9 mg, 0.01 mmol), $Zn(OAc)_2$ (18.3 mg, 0.1 mmol), $In(OAc)_3$ (24.8 mg, 0.085 mmol), 2 mL ODE and 3 mL OAm were mixed in a 50 mL three-neck flask. The mixture was degassed at 100 °C for 20 min, then 1 mL DDT was injected. The sulfur precursor (0.8 mmol sulfur powder dispersed in 2 mL OAm) was swiftly injected into the solution at 220 °C. After reacting for 10 min, the reaction in the solution was stopped by cooling to 100 °C. 0.4 mmol $Zn(OAc)_2$ (in 0.5 mL OAm) was injected, then the temperature was increased to 180 °C for ZnS shell growth. After 10 min, the reaction was stopped by cooling to room temperature. For purification, the CZIS/ZnS NCs were precipitated using hexane and acetone for three times and re-dispersed in hexane for further use.

For the CZIS/ZnS NCs with different ECL emission potential, the amount of CuI was varied by fixing the total amount of $Zn(OAc)_2$ and $In(OAc)_3$ (0.185 mmol) in the initial mixture described above. Specifically, for the CZIS/ZnS NCs samples with ECL emission at −1.11, −1.68, and

−2.10 V vs Ag/AgCl, the amount of CuI was 0.1, 0.01, and 0.001 mmol in precursor, respectively.

Water solubilization of the oil soluble CZIS/ZnS NCs was performed by replacing the initial hydrophobic OAm cladding surfactants with GSH and MPA (Scheme 1A) to aminate and carboxylate the surface of CZIS/ZnS NCs. A mixture of MPA (0.2 mL, ~2 mmol), GSH (23 mg, 0.075 mmol), stoichiometric TMAOH and 100 μL CZIS/ZnS NCs were added into 0.5 mL of N, N-dimethylformamide (DMF) to form an opaque solution. Thereafter, the mixture was heated to 100 °C after deaeration with air and H_2O and then stirred in nitrogen atmosphere. After 20 min, the product was centrifugated at 6000 rpm and washed with EA. The precipitates were dissolved in PBS buffer solution (pH 7.4) for further use.

2.3. Preparation of the ECL probes

Probe 21, probe 141, and probe 155 were prepared via a carboxyl-amino condensation reaction (Scheme 1 B). The each as prepared water soluble CZIS/ZnS NCs samples (100 μL) were activated in the presence of 20 μL (50 mg mL^{-1}) of EDC and 20 μL (50 mg mL^{-1}) of NHS for 20 min then centrifugal at 12000 rpm to remove the excess EDC and NHS. The resultant activated CZIS/ZnS NCs were redispersed in 50 μL Tris-HCl buffer (pH 7.4) and covalently linked with 3′-NH_2 modified hairpin DNA (20 nmol). The reaction was performed by gentle mixing for 3 h. The probes were then purified by ultrafiltration through a 30000 MW size filter at 6000 rpm for 20 min and washed twice with water to remove the nonspecifically bound hairpin DNA and re-dispersed in 20 μL Tris-HCl buffer. Specifically, for the CZIS/ZnS NCs samples ECL emission at −1.11, −1.68, and −2.10 V vs Ag/AgCl, separately link with NH_2-HDNA1-Fc, NH_2-HDNA2-Fc and NH_2-HDNA3-Fc to prepare probe 21, probe 141, and probe 155.

2.4. Fabrication of the ECL biosensor

The GCE was preprocessed by polishing with 0.3 and 0.05 μm α-Al_2O_3 powder successively, then cleaned ultrasonically with ethanol and water and dried at room temperature. First, 4 μL of CS solution was dropped on the surface of the GCE and dried in air to form the CS modified GCE (CS/GCE). Next, the CS/GCE was incubated with 5 μL of GA (5%) at room temperature for 120 min to form GA/CS/GCE. Thereafter, 10 μL isoconcentration mixture (0.33 mM) of probe 21, probe 141, and probe 155 was successively dropped onto the surface of the GA/CS/GCE and incubated at room temperature for 180 min to obtain the probes/GA/CS/GCE. The probes/GA/CS/GCE was incubated with 5 μL of MCH (1 mM) for 30 min to block the unspecific sites. After each step, the electrode was rinsed thoroughly with ultrapure water. The ECL biosensor of the three probes/GA/CS/GCE was obtained.

2.5. ECL measurements

The target miRNAs mixture (10 μL) at different concentrations was dropped onto the ECL biosensor and incubated with the probes at 37 °C for 120 min, followed by a thorough washing with 0.1 M PBS (pH 7.4) to remove unbound target miRNAs. ECL measurements were performed by cyclic voltammetry (CV) method in 0.1 M PBS (pH 7.4) containing 5 mM $K_2S_2O_8$. The scanning potential for ECL was from 0 to −2.30 V, the scanning rate was 0.1 V/s, and the voltage of the photomultiplier tube (PMT) was set at 900 V unless otherwise stated. The concentration of miRNA-21, miRNA-141, and miRNA-155 were quantified by an increase of ECL intensity ΔI ($\Delta I = I_0 - I$) at −1.11, −1.68, and −2.10 V vs Ag/

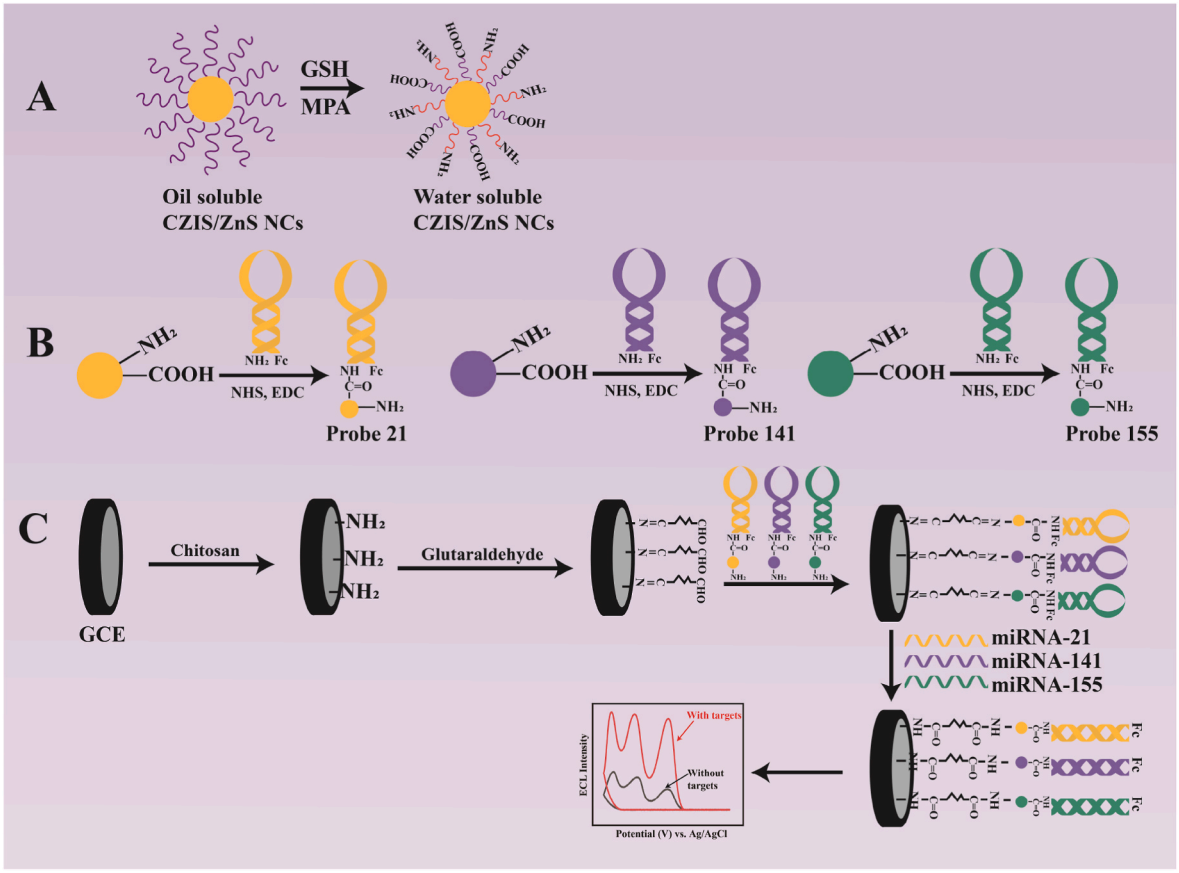

Scheme 1. Schematic illustrations of (A) the ligand exchange process of CZIS/ZnS NCs, (B) procedures of preparation of probe 21, probe 141, and probe 155, (C) the fabricating procedures of ECL biosensor and the detection process.

AgCl, respectively, where I_0 and I is the ECL peak intensity before and after hybridization. All the ECL experiments were performed at room temperature.

3. Results and discussion

3.1. Materials characterization

Transmission electron microscope (TEM) and X-ray diffraction (XRD) were employed to characterize the morphology and structural information of the NCs. As shown in Fig. 1, the TEM photograph indicated that all the three CZIS NCs core the three CZIS/ZnS NCs had a similar particle size with 4.4 nm and 8.6 nm, respectively, which excluded the size effect on the shift of the band edges. The histograms of the size distribution for CZIS and CZIS/ZnS NCs based on the statistical analysis method (more than 200 particles) are shown in Fig. S1 of the Supporting Information. Fig. 1G shows the XRD patterns of CZIS/ZnS NCs. All NCs showed that the diffraction peaks slightly shifted to higher angles with increasing of Cu amount, which reveals that no phase separation and separated nucleation occurred via our method (Torimoto et al., 2007; Zhong et al., 2003). Compared with the standard XRD PDF card of ZnS (JCPDS 65–9585), the XRD characteristic peaks of the NCs were assigned to face-centered cubic (FCC) structure. The lattice spacing of the NCs (0.312 nm), as shown in the inset of Fig. 1D–F can be ascribed to the (1 1 1) planes of the FCC CZIS/ZnS NCs. Moreover, three diffraction rings in the selected area electron diffraction (SAED) pattern can also be indexed to the (1 1 1), (2 2 0), and (3 1 1) planes, respectively, which agreed with the results of the corresponding XRD pattern (Fig. S2). The chemical compositions of the resulting CZIS/ZnS NCs samples were determined using ICP-MS (Table S1). The Cu/Zn atomic ratios were calculated based on ICP-MS data and compared with the nominal values. It can be seen that the real Cu/Zn ratios in the as prepared CZIS/ZnS NCs samples were slight lower than those of the nominal values. This is the result of the different chemical reactivities of the Cu and Zn precursors.

Fig. 2A and B shows the ultraviolet–visible (UV–Vis) absorption and FL emission spectra of CZIS/ZnS NCs prepared by changing molar ratios of Cu precursor. The absorption band edges and FL spectra of the CZIS/ZnS NCs red-shifted from 350 to 635 nm and 436–730 nm with increasing the molar of Cu from 0.001 to 0.1 mmol, respectively. Given that the similar particle size of three CZIS and CZIS/ZnS NCs, the red-shift of UV–Vis absorption and FL spectra of CZIS/ZnS NCs could be attributed to the increasing of ratios of Cu in the composition of the CZIS/ZnS NCs (Zhang et al., 2011). In addition, as shown in Fig. 2B, all the FL peak wavelength and the FL spectra shape of NCs did not undergo observable change after the process of ligand exchange (Fig. 2B, dotted curves). The FL intensity of as prepared water-soluble CZIS/ZnS NCs was only slightly decreased about 10% compared to that of the original oil-soluble samples, this attribute to the passivation effect of the ZnS shell (Fig. 2B, dotted curves). Under UV light excitation (365 nm), three bright FL colors (blue, red, and deep red) are observed from the luminescence photos of three CZIS/ZnS NCs in both oil and aqueous phase

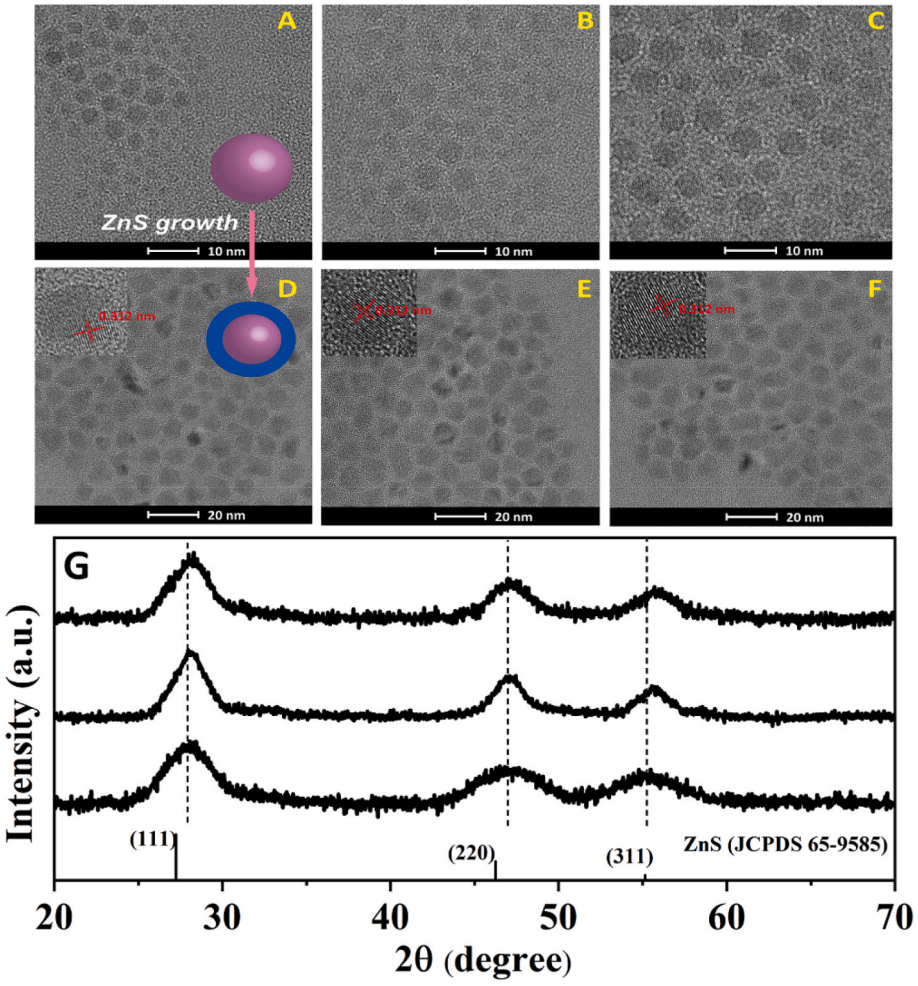

Fig. 1. TEM images of three kinds of CZIS NCs before (A)–(C) and after (D)–(F) epitaxial growth of ZnS shell. (G) XRD patterns of the three CZIS/ZnS NCs samples, the curve from top to bottom correspond to (D)–(F) and represent 0.001 mmol, 0.01 mmol, and 0.1 mmol Cu in precursor.

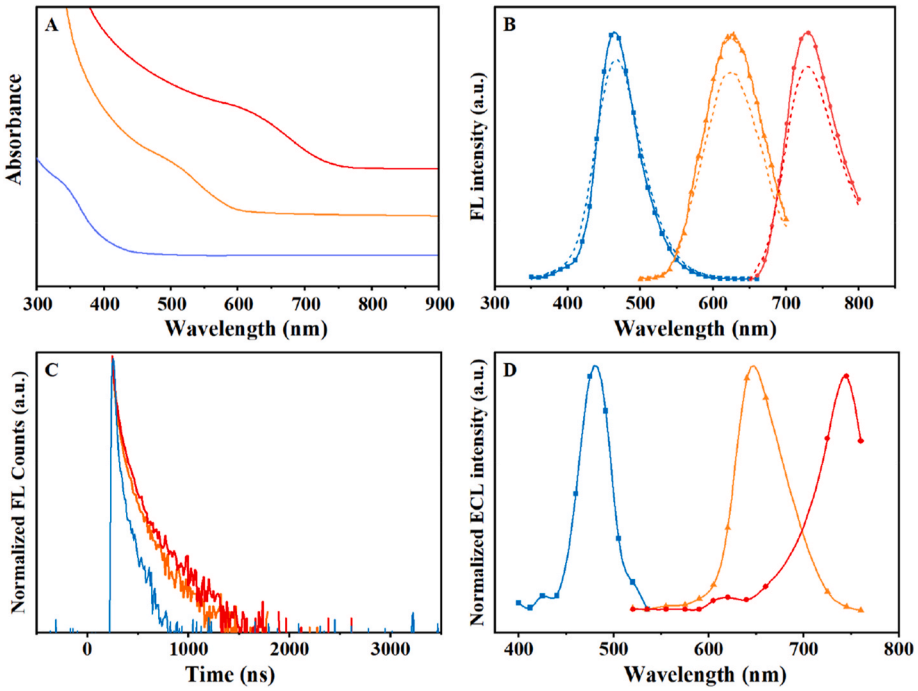

Fig. 2. (A) UV–Vis absorption and (B) FL spectra before (solid curve) and after (dotted curve) ligand exchange of CZIS/ZnS NCs, (C) FL decay curves of CZIS/ZnS NCs. (D) ECL spectra. (Blue, orange and red curve represent the CZIS/ZnS NCs containing 0.001 mmol, 0.01 mmol, and 0.1 mmol Cu in precursor). (For interpretation of the references to color in this figure legend, the reader is referred to the Web version of this article.)

solution (Fig. S3). Fig. 2C shows the time-resolved FL spectra, the FL excited-state lifetime prolonged with the increasing of the Cu ratio in the NCs, and located in the range of hundreds of nanoseconds (120–756 ns, details list in Table S2), which means the FL emission originated from the Cu dopant transition (Zhang et al., 2014). Fig. S4 summarizes the FL intensity and peak wavelength in the FL emission spectra of the resulting CZIS/ZnS NCs with the variation Cu contents, and the maximum of Φ_{FL} of 75% of the samples were determined via using tris(2,2′-bipyridine) ruthenium dichloride (4% in air saturated aqueous solution).

Fourier transform infrared spectroscopy (FTIR) spectra were then employed to analyze the nature of the surface groups of the CZIS/ZnS NCs before and after ligand exchange with MPA and GSH (Fig. S5). Before ligand exchange, two sharp and strong absorption peaks at 2840 and 2959 cm^{-1} represent the stretching vibration of the C–H bond from OAm. The peaks at 1530, 1450, and 1405 cm^{-1} are characteristic of $–CH_3$ absorption, and the peak at 720 cm^{-1} corresponds to the bending vibration of $-(CH_2)_n-$ vibration from OAm (blue curve). In contrast, the characteristic peaks above OAm weakened markedly as the CZIS/ZnS NCs after ligand exchange with MPA and GSH (red curve). In addition, it was found that the CZIS/ZnS NCs after ligand exchange had a broad peak at 3450 cm^{-1}, which can be assigned to the O–H bond stretching vibration of –COOH groups from MPA and GSH. In contrast, the OAm capped CZIS/ZnS NCs before ligand exchange did not record any vibration signal of –COOH. The N–H bond stretching vibration from $–NH_2$ of GSH was covered by the broad and strong –COOH absorption peak; only a bulge band can be observed at 3250 cm^{-1}; however, the vibration in the plane of N–H bond of GSH can be clearly observed at 1650 cm^{-1}. Thus, the FTIR spectra provide evidence of a successful ligand exchange process on the surface of CZIS/ZnS NCs. The ECL probes also was characterized by using FTIR (Fig. S6). Furthermore, the CZIS/ZnS NCs also exhibited a good crystalline structure after the ligand exchange process (Fig. S7). These observations, combined with a wide range peak shift in the UV–Vis absorption and FL spectra, confirmed the successful preparation of the CZIS/ZnS NCs with a large tunable bad gap.

3.2. ECL mechanism

Fig. 3A and Fig. 3B show the cyclic voltammograms (CVs) and ECL behaviors of three CZIS/ZnS NCs samples separately modified GCE (curves a-c) in 0.1 M N_2-saturated PBS (pH 7.4) upon negative scanning from 0 to −2.30 V. At CZIS/ZnS NCs samples modified GCE, the onset potential and reduction peaks are gradually shifted to a more positive potential with the Cu ratio increasing and onset potential observed at −1.80, −1.50, and −0.75 V vs. Ag/AgCl, reduction peaks observed at −2.10, −1.68, and −1.11 V vs. Ag/AgCl, respectively (Fig. 3A). The three reduction peaks could be assigned to the CZIS/ZnS NCs electrochemically reduced to negative charge states (CZIS/ZnS $NCs^{\bullet-}$, anionic radical) by injecting electrons into the conduction band of CZIS/ZnS NCs [Eq. (1)]. As the same time, there was no obvious ECL emission peak (Fig. 3B). Fig. 3C shows the CVs of the three CZIS/ZnS NCs samples separately modified GCE (curves a-c), the mixed CZIS/ZnS NCs samples modified GCE (curve d), and bare GCE (curve e) in 0.1 M PBS (pH 7.4) containing 5 mM $S_2O_8^{2-}$ as a coreactant. $S_2O_8^{2-}$ displayed a strong and broad reduction current on a bare GCE with an onset around −0.52 V and a maximum response of approximately −1.11 V, and no obvious ECL was detected (Fig. 3D, curve e). Correspondingly, in the in the presence of $S_2O_8^{2-}$, the CVs of the three CZIS/ZnS NCs samples and the mixed samples separately modified GCE displayed cathodic reduction and the reduction potential peak in keeping with the absence $S_2O_8^{2-}$ (Fig. 3A). Fig. 3D shows the ECL behaviors of the three CZIS/ZnS NCs samples separately modified GCE (curves a-c) and mixed samples modified GCE (curve d) in the presence of $S_2O_8^{2-}$. Compared with the absence of $S_2O_8^{2-}$, a strong ECL signal was obtained in the presence of $S_2O_8^{2-}$at the three prepared CZIS/ZnS NCs samples separately modified GCE. The ECL peak potentials were consistent with their CV reduction peaks. Moreover, the mixed CZIS/ZnS NCs samples modified GCE also produced three separated ECL peaks, indicating its promising application in potential-resolved ECL detection at a single cathode ECL process. In the $S_2O_8^{2-}$ electrochemical reduction process, the $S_2O_8^{2-}$ was electrochemically reduced to a strong oxidizing free radical $SO_4^{\bullet-}$ [Eq. (2)], which could oxidize CZIS/ZnS $NCs^{\bullet-}$ by injecting holes into the valence

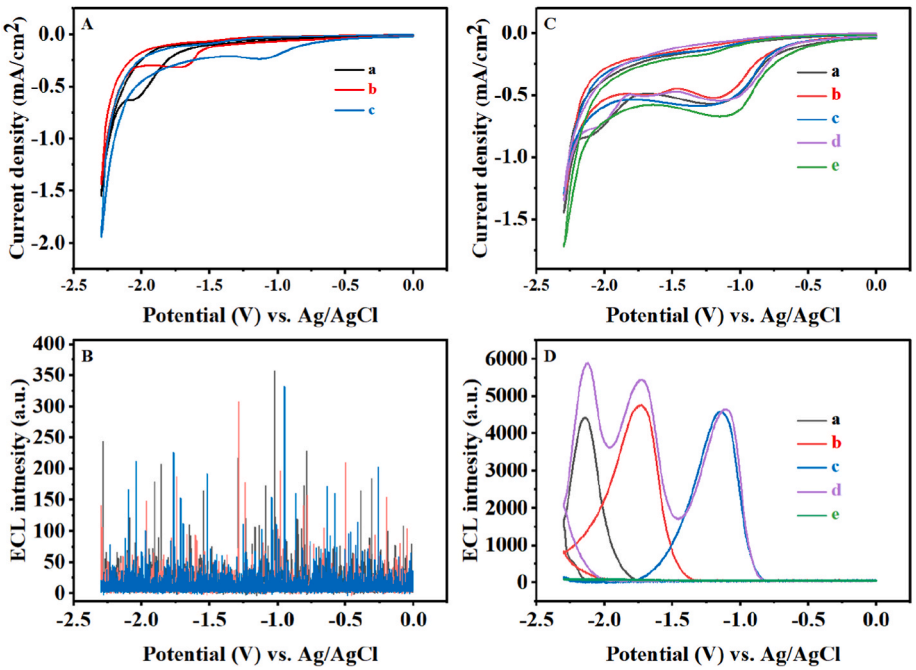

Fig. 3. (A) CVs and (B) ECL behaviors of three CZIS/ZnS NCs modified GCE (curves a-c) in 0.1 M N_2-saturated PBS (pH 7.4, PMT = 600 V). (C) CVs and (D) ECL behaviors of three CZIS/ZnS NCs respectively modified GCE (curves a-c), the mixed sample modified GCE (curve d) and bare GCE (curve e) in 0.1 M PBS (pH 7.4) containing 5 mM $K_2S_2O_8$ (pH 7.4), CVs scanning potential from 0 to −2.30 V at a scanning rate of 0.1 V/s, PMT = 600 V. Black, red and blue curve represent the CZIS/ZnS NCs containing 0.001, 0.001, and 0.1 mmol Cu in precursor, respectively. (For interpretation of the references to color in this figure legend, the reader is referred to the Web version of this article.)

band of CZIS/ZnS NCs$^{\bullet-}$ and formed excited states CZIS/ZnS NCs* [Eq. (3)]. Then, the CZIS/ZnS NCs* return to the ground state by emit light [Eq. (4)]. In addition, the ECL spectra emission peaks of the three samples separately located at 480, 646, and 742 nm exhibited red shifts of 44, 21, and 12 nm, respectively, in comparison with their FL emission peaks (Fig. 2D). The red shifted ECL emission indicated that the ECL emission for the three CZIS/ZnS NCs samples was derived from the surface state transitions instead of the band gap transition (Ding et al., 2002; Poznyak et al., 2004). Based on the analysis above, the ECL mechanism of the CZIS/ZnS NCs in the presence of $S_2O_8^{2-}$ can be identified as a typical reductive-oxidative ECL mechanism (Ding et al., 2002; Poznyak et al., 2004) and proposed as follows:

$$\text{CZIS/ZnS NCs} + e^- \rightarrow \text{CZIS/ZnS NCs}^{\bullet-} \quad (1)$$

$$S_2O_8^{2-} + e^- \rightarrow SO_4^{2-} + SO_4^{\bullet-} \quad (2)$$

$$\text{CZIS/ZnS NCs}^{\bullet-} + SO_4^{\bullet-} \rightarrow \text{CZIS/ZnS NCs*} + SO_4^{2-} \quad (3)$$

$$\text{CZIS/ZnS NCs*} \rightarrow \text{CZIS/ZnS NCs} + h\nu \quad (4)$$

3.3. Characterizations of the ECL biosensor

The fabrication process of the potential-resolved ECL biosensor was implemented according to Scheme 1C, and the ECL biosensor fabricated was characterized by electrochemical impedance spectroscopy (EIS) in 0.1 M (pH 7.4) PBS including 5 mM $[Fe(CN)_6]^{3-/4-}$ and 0.1 M KCl (Fig. 4). According to Fig. 4, the bare GCE exhibited a minimum electron-transfer resistance (R_{et}) value of approximately 100 Ω (curve a) and an almost straight line, which indicates the good mass-transfer property of GCE and a diffusion-controlled process (Bai et al., 2019). Compared with bare GCE (curve a), after the modification of CS and GA on the electrode successively, EIS revealed an increased R_{et} value (curves b and c), which was attributed to the low conductivity of CS and GA. When a mixture of probe 21, probe 141, and probe 155 bonded with GA/CS/GCE, it exhibited a significantly increased R_{et} (curve d) owing to the increase in electrostatic repulsion between the negatively charged DNA probes and the $[Fe(CN)_6]^{3-/4-}$pair. Also, after MCH blocked the modified electrode surface, EIS showed an increased R_{et} for the

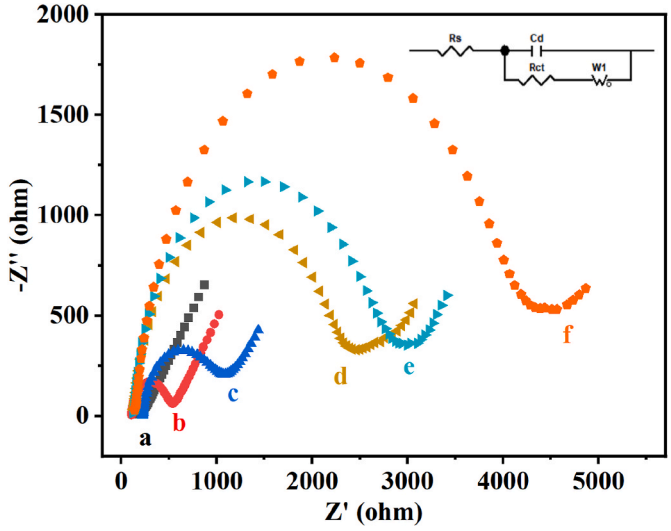

Fig. 4. EIS curves for the stepwise biosensor fabrication measured in 5.0 mM $[Fe(CN)_6]^{3-/4-}$ containing 0.1 M KCl at different modified electrodes: (a) bare GCE, (b) CS/GCE, (c) GA/CS/GCE, (d) three probes/GA/CS/GCE, (e) three probes/MCH/GA/CS/GCE, (f) the three probes/MCH/GA/CS/GCE incubation target miRNA-21, miRNA-141, and miRNA-155 mixture sample, inset: equivalent circuit of the biosensor.

hindrance effect on the $[Fe(CN)_6]^{3-/4-}$pair diffusion by the compact self-assembly MCH layer (curve e). When the biosensor was incubated with target miRNA mixture samples of miRNA-21, miRNA-141, and miRNA-155 (curve f), the electron transfer became more difficult, and the R_{et} significantly increased. This results from the successful incubation of the target miRNAs with the biosensor, causing the fold probes to convert into a linear double-helix configuration and an increase in the interfacial barrier for the diffusion of $[Fe(CN)_6]^{3-/4-}$. The above results indicate the successful preparation of the proposed potential-resolved multi-object detection ECL biosensor.

The simultaneous detection capability of our sensor for miRNA-21, miRNA-141, and miRNA-155 was verified as shown in Fig. 5. Curve a

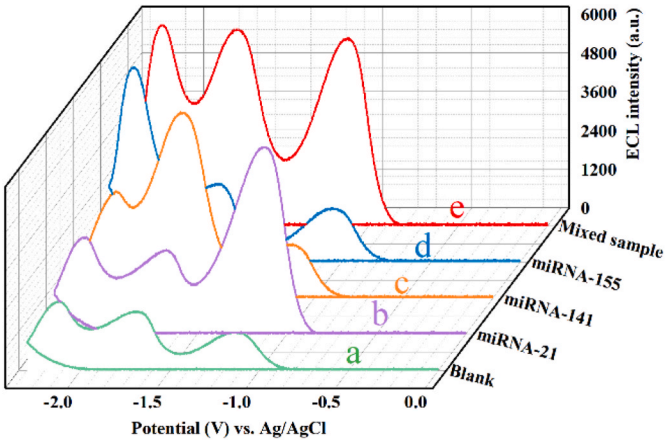

Fig. 5. The ECL response profiles of (a) blank solution, (b) miRNA-21 (1 nM), (c) miRNA-141(1 nM), (d) miRNA-155 (1 nM), and (e) isoconcentration mixed sample of miRNA-21, miRNA-141, and miRNA-155 (1 nM). ECL signals were measured in the solution containing 5 mM $K_2S_2O_8$ by scanning the potential from 0 to −2.30 V at a scanning rate of 0.1 V/s and PMT = 900 V.

displayed the ECL-Potential profile of the incubation of the blank solution with the biosensor, which shown three ECL peak at different potential positions (−2.10, −1.68, and −1.11 V vs. Ag/AgCl) and an obviously decrease compared with the three CZIS/ZnS NCs mixture sample modified GCE in Fig. 3D curve e even at higher PMT voltage. This is because the three probes were in the folded configuration and Fc was held in close proximity to the CZIS/ZnS NCs, which confirmed that Fc effectively quenched the ECL of CZIS/ZnS NCs. Curve b shown the incubation of the target miRNA-21 (1 nM) with the biosensor, which leads to significant increase in ECL intensity response at −1.11 V, while the peak at −1.68 and −2.10 V corresponding to probe 141 and probe 155 remains unchanged. This means that probe 21 was opened and converted into a linear double-helix configuration by hybridizing with miRNA-21, which resulted in the Fc moving away from the CZIS/ZnS NCs and an increased ECL intensity. Similarly, the alone incubation of the target miRNA-141 (1 nM) or miRNA-155 (1 nM), results in the increase of ECL intensity peak at −1.68 or −2.10 V, and the ECL peak of −1.11, −2.10 V in curve c and ECL peak of −1.11, −1.68 V in curve d is not affected (curves c and d). This comparison indicates that our biosensor can be employed to distinguish and detect either miRNA-21, miRNA-141, or miRNA-155. More importantly, when triple miRNA-21, miRNA-141, and miRNA-155 are incubated with the biosensor, simultaneous and significant increase in ECL intensity responses for the three peaks at −1.11, −1.68, and −2.10 V vs Ag/AgCl are observed (curve e), which indicated the feasibility of our potential-resolved ECL biosensor for the simultaneous detection of miRNA-21, miRNA-141, miRNA-155 at a single cathodic ECL process. In addition, the successful recovery of ECL intensity after incubation with target miRNAs confirmed that the CZIS/ZnS NCs modified hairpin probes were successfully immobilized onto the GCE and the hairpin DNA preserved its bioreactivity after the functionalization with CZIS/ZnS NCs.

3.4. Analytical performance of the ECL biosensor for target miRNAs

Under the optimized conditions, the biosensor was employed for simultaneous detection of miRNA-21, miRNA-141, and miRNA-155, and the ECL signals of various concentrations of analyte miRNA were recorded to evaluate the biosensor simultaneous detection performance. As shown in Fig. 6A, upon increasing miRNA-21, miRNA-141, and miRNA-155 concentrations in the mixture sample, the ECL intensities gradually increased. The calibration plots (Fig. 6B–D) displayed a good positive linear relationship between the ECL response intensity and the logarithmic concentrations of miRNA-21, miRNA-141, and miRNA-155 in the range of 0.00001 nM–10 nM, 0.00001 nM–10 nM and 0.00001 nm–10 nM, respectively. Furthermore, the linear regression equations were $\Delta I_{ECL} = 681.2\lg c_{miRNA\text{-}21}+3913$ with a squared correlation coefficient (R^2) of 0.996 for miRNA-21, and $\Delta I_{ECL} = 557.8\lg c_{miRNA\text{-}141}+3373$ with an R^2 of 0.992 for miRNA-141 and $\Delta I_{ECL} = 547.7\lg c_{miRNA\text{-}155}+3296$ with an R^2 of 0.997 for miRNA-155. Moreover, the limit of detection (LOD) was evaluated to be 2.2, 2.6, and 2.7 fM for miRNA-21, miRNA-

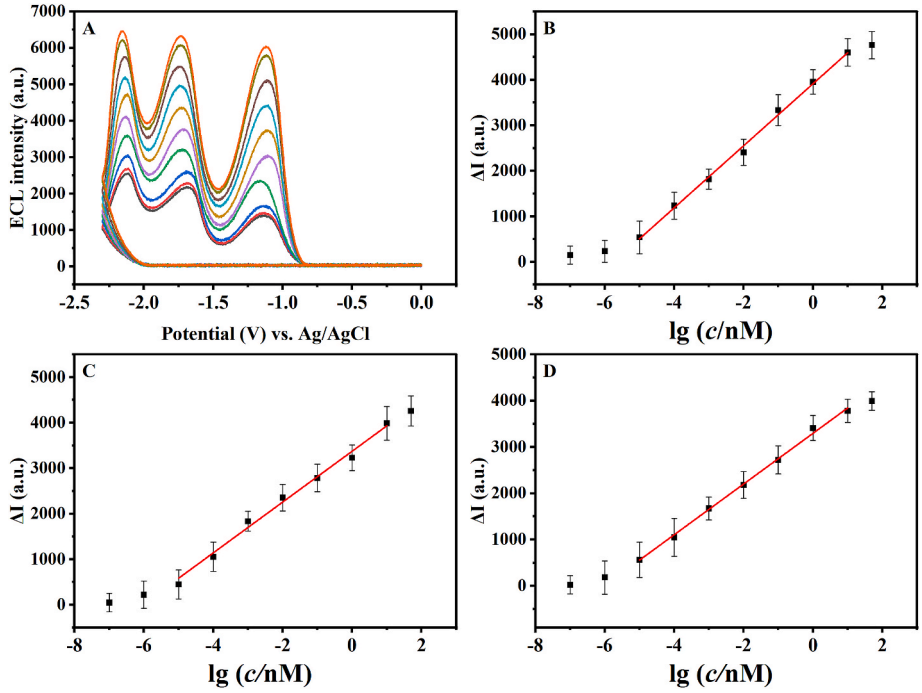

Fig. 6. (A) ECL-Potential profiles of biosensor formed with isoconcentration mixed sample of miRNA-21, miRNA-141, and miRNA-155, (a) blank, (b) 0.000001 nM, (c) 0.00001 nM, (d) 0.0001 nM, (e) 0.001 nM, (f) 0.01 nM, (g) 0.1 nM, (h) 1 nM, (i) 10 nM, (j) 50 nM. (B)–(D) Corresponding calibration curve for determining miRNA-21, miRNA-141, and miRNA-155, respectively. The ECL measurement conditions are the same as those in Fig. 5.

141, and miRNA-155 at a condition of signal to noise ratio (S/N) of 3. Six repetitive measurements of miRNA-21, miRNA-141, and miRNA-155 at 1 nM yielded relative the standard deviations of 5.6%, 6.7%, and 7.0%, respectively, indicating good reproducibility of the biosensor. The ECL biosensor was further compared with the recently reported electrochemical (Chang et al., 2019; Fu et al., 2020), fluoresce (Gao et al., 2019), and ECL sensors (Feng et al., 2016; Wang et al., 2021a) for the simultaneous detection multiple miRNAs listed in Table S3. The result indicated that the detection limit of our biosensor for miRNA-21, miRNA-141, and miRNA-155 showed a relatively low detection limit. In addition, compared with other ECL sensors, our sensor only required measurement at a single cathodic ECL process to simultaneous detect three kinds of miRNA with only one coreactant component.

As a result of less base pairing and high sequence homology among miRNA families, the selectivity determining target miRNA is a great challenge. The normal interfering miRNAs in the body of miRNA-205, miRNA-429 and miRNA-101 with 10-fold concentration (100 pM) were compared to evaluate the selectivity of biosensor for miRNA-21, miRNA-141, and miRNA-155. The fabricated biosensor displayed strong ECL intensity increasing responses to 10 pM miRNA-21, miRNA-141, and miRNA-155, whereas the ECL signals of the interfering miRNAs were much closer to the blank solution (Fig. S8). In addition, the mixture sample of the target miRNA and the interfering miRNAs also displayed high increased ECL intensity on the verge of ECL responses of each target miRNA. This reveals that the interfering miRNAs displayed a negligible effect on the biosensor, and the selectivity of the as-prepared ECL biosensor was, therefore, evident.

4. Conclusions

In summary, the ECL emission potential tunable CZIS/ZnS NCs were synthesized with non-toxic elements and investigated for the first time, which provides a promising candidate for ECL luminophores in the field of multiple signal ECL sensor systems. As a result, the CZIS/ZnS NCs exhibited efficient ECL emission in the presence of $S_2O_8^{2-}$, and the ECL emission potential can be tuned from −2.10 to −1.11 V by changing the ratio of Cu in precursor. In addition, a potential-resolved ECL biosensor was fabricated based on the prepared CZIS/ZnS NCs for the simultaneous detection of three miRNAs in a single cathodic ECL process. That simplified the multiple signal ECL sensor system with fewer coreactant components and electrochemical processes. Moreover, the results illustrate the promise of CZIS/ZnS NCs for sensitive and multiobjective bioassays and provide new avenues for potential-resolved multi-object detection ECL system construction and the development of novel non-toxic element NCs-based ECL luminophores.

CRediT authorship contribution statement

Yang Jiang: Conceptualization, Methodology, Data curation, Writing – original draft, Writing – review & editing. **Qian Li:** Investigation, Data curation, Formal analysis, Writing – review & editing. **Yun Xu:** Investigation, Formal analysis, Writing – review & editing. **Wanqiao Bai:** Investigation, Data curation, Formal analysis, Writing – review & editing. **Xia Yang:** Methodology, Validation, Formal analysis, Methodology, Writing – review & editing. **Sijia Li:** Methodology, Validation, Formal analysis, Methodology, Writing – review & editing. **Yan Li:** Supervision, Project administration, Conceptualization, Methodology, Writing – review & editing.

Declaration of competing interest

The authors declare that they have no known competing financial interests or personal relationships that could have appeared to influence the work reported in this paper.

Acknowledgements

This work was supported by the National Natural Science Foundation of China (No. 22074119, 21675124, 21375102), the National Key R&D Program of China (No. 2019YFD1002405) and the Natural Science Basic Research Program of Shaanxi (No. 2020JM-426).

Appendix A. Supplementary data

Supplementary data to this article can be found online at https://doi.org/10.1016/j.bios.2022.113980.

References

Babamiri, B., Hallaj, R., Salimi, A., 2018. Biosens. Bioelectron. 99, 353–360.
Bai, W., Cui, A., Liu, M., Qiao, X., Li, Y., Wang, T., 2019. Anal. Chem. 91 (18), 11840–11847.
Bartel, D.P., 2018. Cell 173 (1), 20–51.
Cao, Z., Shu, Y., Qin, H., Su, B., Peng, X., 2020. ACS Cent. Sci. 6 (7), 1129–1137.
Chang, J., Wang, X., Wang, J., Li, H., Li, F., 2019. Anal. Chem. 91 (5), 3604–3610.
Coughlan, C., Ibanez, M., Dobrozhan, O., Singh, A., Cabot, A., Ryan, K.M., 2017. Chem. Rev. 117 (9), 5865–6109.
Deiss, F., LaFratta, C.N., Symer, M., Blicharz, T.M., Sojic, N., Walt, D.R., 2009. J. Am. Chem. Soc. 131 (17), 6088–6091.
Ding, Z.F., Quinn, B.M., Haram, S.K., Pell, L.E., Korgel, B.A., Bard, A.J., 2002. Science 296 (5571), 1293–1297.
Feng, X., Gan, N., Zhang, H., Li, T., Cao, Y., Hu, F., Jiang, Q., 2016. Biosens. Bioelectron. 75, 308–314.
Feng, X., Gan, N., Zhang, H., Yan, Q., Li, T., Cao, Y., Hu, F., Yu, H., Jiang, Q., 2015. Biosens. Bioelectron. 74, 587–593.
Fu, P., Xing, S., Xu, M., Zhao, Y., Zhao, C., 2020. Sensor. Actuator. B Chem. 305, 127545.
Gao, H., Li, J., Jia, Y., Yu, X., Qi, J., Tian, J., Yu, B., 2019. Analyst 144 (24), 7178–7184.
Gebert, L.F.R., MacRae, I.J., 2019. Nat. Rev. Mol. Cell Biol. 20 (1), 21–37.
Guo, W., Ding, H., Gu, C., Liu, Y., Jiang, X., Su, B., Shao, Y., 2018. J. Am. Chem. Soc. 140 (46), 15904–15915.
Han, F., Jiang, H., Fang, D., Jiang, D., 2014. Anal. Chem. 86 (14), 6896–6902.
Jones, A., Dhanapala, L., Kankanamage, R.N.T., Kumar, C.V., Rusling, J.F., 2020. Anal. Chem. 92 (1), 345–362.
Knowles, K.E., Hartstein, K.H., Kilburn, T.B., Marchioro, A., Nelson, H.D., Whitham, P.J., Gamelin, D.R., 2016. Chem. Rev. 116 (18), 10820–10851.
Li, L., Pandey, A., Werder, D.J., Khanal, B.P., Pietryga, J.M., Klimov, V.I., 2011. J. Am. Chem. Soc. 133 (5), 1176–1179.
Liu, W., Chen, A., Li, S., Peng, K., Chai, Y., Yuan, R., 2019. Anal. Chem. 91 (2), 1516–1523.
Lv, W., Ye, H., Yuan, Z., Liu, X., Chen, X., Yang, W., 2020. Trends Anal. Chem. 123, 115767–115776.
Ma, C., Cao, Y., Gou, X.D., Zhu, J.J., 2020. Anal. Chem. 92 (1), 431–454.
Ma, Z., Liu, N., 2015. Expert Rev. Mol. Diagn. 15 (8), 1075–1083.
Owens, J., Brus, L., 2017. J. Am. Chem. Soc. 139 (32), 10939–10943.
Pakchin, P.S., Nakhjavani, S.A., Saber, R., Ghanbari, H., Omidi, Y., 2017. Trends Anal. Chem. 92, 32–41.
Pan, D., An, L., Sun, Z., Hou, W., Yang, Y., Yang, Z., Lu, Y., 2008. J. Am. Chem. Soc. 130 (17), 5620–5621.
Poznyak, S.K., Talapin, D.V., Shevchenko, E.V., Weller, H., 2004. Nano Lett. 4 (4), 693–698.
Pu, C., Ma, J., Qin, H., Yan, M., Fu, T., Niu, Y., Yang, X., Huang, Y., Zhao, F., Peng, X., 2016. ACS Cent. Sci. 2 (1), 32–39.
Qi, H., Zhang, C., 2020. Anal. Chem. 92 (1), 524–534.
Stroyuk, O., Raevskaya, A., Gaponik, N., 2018. Chem. Soc. Rev. 47 (14), 5354–5422.
Sun, Y., Wu, X., Zhang, K., Ren, Q., Xie, R., 2018. Biosens. Bioelectron. 100, 445–452.
Thorsson, V., Gibbs, D.L., Brown, et al., 2018. Immunity 48 (4), 812–830.
Torimoto, T., Adachi, T., Okazaki, K., Sakuraoka, M., Shibayama, T., Ohtani, B., Kudo, A., Kuwabata, S., 2007. J. Am. Chem. Soc. 129 (41), 12388–12389.
Treiber, T., Treiber, N., Meister, G., 2019. Nat. Rev. Mol. Cell Biol. 20 (1), 5–20.
Wang, F., Liu, Y., Fu, C., Li, N., Du, M., Zhang, L., Ge, S., Yu, J., 2021a. Anal. Chem. 93 (3), 1702–1708.
Wang, N., Chen, L., Chen, W., Ju, H., 2021b. Anal. Chem. 93 (12), 5327–5333.
Wu, P., Yan, X., 2013. Chem. Soc. Rev. 42 (12), 5489–5521.
Ye, J., Liu, G., Yan, M., Zhu, Q., Zhu, L., Huang, J., Yang, X., 2019. Anal. Chem. 91 (20), 13237–13243.
Zhang, B., Zhang, F., Zhang, P., Shen, D., Gao, X., Zou, G., 2019a. Anal. Chem. 91 (5), 3754–3758.
Zhang, J., Arbault, S., Sojic, N., Jiang, D., 2019b. Annu. Rev. Anal. Chem. 12, 275–295.
Zhang, J., Xie, R., Yang, W., 2011. Chem. Mater. 23 (14), 3357–3361.
Zhang, W., Lou, Q., Ji, W., Zhao, J., Zhong, X., 2014. Chem. Mater. 26 (2), 1204–1212.
Zhang, Y., Xu, G., Lian, G., Luo, F., Xie, Q., Lin, Z., Chen, G., 2020. Biosens. Bioelectron. 164, 112332.
Zhong, X., Han, M., Dong, Z., White, T.J., Knoll, W., 2003. J. Am. Chem. Soc. 125 (28), 8589–8594.

Zhou, B., Zhu, M., Hao, Y., Yang, P., 2017. ACS Appl. Mater. Interfaces 9 (36), 30536–30542.
Zhou, J., Nie, L., Zhang, B., Zou, G., 2018. Anal. Chem. 90 (21), 12361–12365.
Zou, G., Tan, X., Long, X., He, Y., Miao, W., 2017. Anal. Chem. 89 (23), 13024–13029.